Journal of Colloid and Interface Science 664 (2024) 667–680

Contents lists available at ScienceDirect

Journal of Colloid And Interface Science

journal homepage: www.elsevier.com/locate/jcis

Regular Article

Efficient green Cr(VI) adsorbent from sorghum waste: Eco-designed functionalized mesoporous silica FDU-12

Saeed Shirazian [a,b,*], Thoa Huynh [c,d], Niloofar Pirestani [e], Roozbeh Soltani [f], Azam Marjani [f], Ahmad B. Albadarin [g], Shaheen M. Sarkar [h]

[a] Institute of Research and Development, Duy Tan University, Da Nang, Vietnam
[b] School of Engineering & Technology, Duy Tan University, Da Nang, Vietnam
[c] Institute for Research and Training in Medicine, Biology and Pharmacy, Duy Tan University, Da Nang, Vietnam
[d] School of Medicine & Pharmacy, Duy Tan University, Da Nang, Vietnam
[e] Department of Environmental Science, Faculty of Agriculture and Natural Resources, Islamic Azad University of Khorasgan, Khorasgan, Isfahan, Iran
[f] Department of Chemistry, Islamic Azad University, Arak Branch, Arak, Iran
[g] B&WB Department of Chemical Engineering and Advanced Energy, American University of Beirut, Beirut, Lebanon
[h] Department of Applied Science, Technological University of the Shannon, Moylish, Limerick V94 EC5T, Ireland

HIGHLIGHTS

- Eco-design of a highly efficient Cr(VI) adsorbent with bimodal micro-/mesoporous structure.
- Green synthesis approach utilizing Sorghum waste as a sustainable silica source for the adsorbent.
- A one-pot synthesis method led to homogeneously distributed adsorption sites on the MI-Cl-FDU-12.
- MI-Cl-FDU-12 demonstrated a high adsorption capacity of 416.9 mg g-1 at 313 K for Cr(VI)
- MI-Cl-FDU-12 adsorbent revealed excellent regeneration performance by six consecutive cycles.

GRAPHICAL ABSTRACT

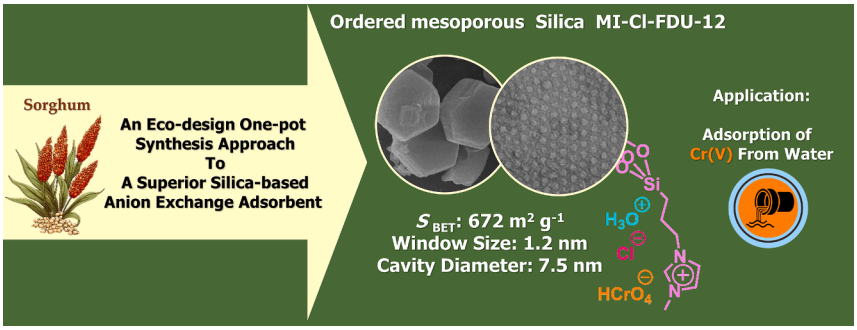

ARTICLE INFO

Keywords:
Cr(VI) adsorption
Eco-design
One-pot synthesis
Mesoporous FDU-12
Sorghum waste

ABSTRACT

This paper presents an eco-design approach to the synthesis of a highly efficient Cr(VI) adsorbent, utilizing a positively charged surface mesoporous FDU-12 material (designated as MI-Cl-FDU-12) for the first time. The MI-Cl-FDU-12 anion-exchange adsorbent was synthesized *via* a facile one-pot synthesis approach using sodium silicate extracted from sorghum waste as a green silica source, 1-methyl-3-(triethoxysilylpropyl) imidazolium chloride as a functionalization agent, triblock copolymer F127 as a templating or pore-directing agent, trimethyl benzene as a swelling agent, KCl as an additive, and water as a solvent. The synthesis method offers a sustainable and environmentally friendly approach to the production of a so-called "green" adsorbent with a bimodal micro-/mesoporous structure and a high surface area comparable with the previous reports regarding FDU-12 synthesis. MI-Cl-FDU-12 was applied as an anion exchanger for the adsorption of toxic Cr(VI) oxyanions from aqueous media and various kinetic and isotherm models were fitted to experimental data to propose the adsorption behavior of Cr(VI) on the adsorbent. Langmuir model revealed the best fit to the experimental data at

* Corresponding author at: Saeed Shirazian, Institute of Research and Development, Duy Tan University, Da Nang, Vietnam.
E-mail address: saeedshirazian@duytan.edu.vn (S. Shirazian).

https://doi.org/10.1016/j.jcis.2024.03.030
Received 28 November 2023; Received in revised form 12 February 2024; Accepted 5 March 2024
Available online 7 March 2024

four different temperatures, indicating a homogeneous surface site affinity. The theoretical maximum adsorption capacities of the adsorbent were found to be 363.5, 385.5, 409.0, and 416.9 mg g^{-1} at 298, 303, 308, and 313 K, respectively; at optimal conditions (pH=2, adsorbent dose=3.0 mg, and contact time of 30 min), surpassing that of most previously reported Cr(VI) adsorbents in the literature. A regeneration study revealed that this adsorbent possesses outstanding performance even after six consecutive recycling.

Nomenclature

Symbols

α	The initial adsorption rate (mg g^{-1} min^{-1})
β	The Elovich adsorption constant (g mg^{-1})
b_t	Temkin isotherm constant related to the heat of adsorption (J mol^{-1})
C_e	The concentration at equilibrium (mg L^{-1})
C_i	Initial concentration (mg L^{-1})
C_t	The concentration at any time t (mg L^{-1})
K_F	Freundlich constant ((mg g^{-1}) (L $mg^{-1})^{1/n}$)
K_L	Langmuir isotherm constant (L mg^{-1})
K_T	Temkin isotherm binding constant (L g^{-1})
k_1	The PFO rate constant (min^{-1})
k_2	The PSO rate constant (g mg^{-1} min^{-1})
$k_{Av.}$	The Avrami kinetic constant (min^{-1})
$n_{Av.}$	The Avrami exponent (unitless)
n	Freundlich constant (unitless)
Q_e	Adsorption capacity at equilibrium (mg g^{-1})
$Q_{e,cal.}$	Calculated equilibrium adsorption capacity (mg g^{-1})
$Q_{e,exp.}$	Experimental equilibrium adsorption capacity (mg g^{-1})
$Q_{m,cal.}$	Langmuir maximum adsorption capacity (mg g^{-1})
Q_t	Adsorption capacity at any time t (mg g^{-1})
R	The universal gas constant (J mol^{-1} K^{-1})
$R^2_{Adj.}$	The adjusted coefficient of determination
t	Time (min)
T	Temperature (K)
V	The volume of solution (mL)
W	Adsorbent dose (mg)

Abbreviations

BET	Brunauer–Emmett–Teller
2D-NLDFT PSD	Two-dimensional nonlocal density functional theory pore size distribution
CPTES	3-chloropropyltriethoxysilane
CrO_4^{2-}	Chromate ion
$Cr_2O_7^{2-}$	Dichromate ion
DDW	Double distilled water
F127	Tri-block copolymer $EO_{106}PO_{70}EO_{106}$ [where EO is poly (ethylene oxide) and PO is poly(propylene oxide)]
FAO	The Food and Agriculture Organization
FESEM	Field emission scanning electron microscopy
FTIR	Fourier transform infrared
HCl	Hydrochloric acid
$HCrO_4^-$	hydrogen chromate ion
ICP-OES	Inductively coupled plasma optical emission spectrometry
$K_2Cr_2O_7$	Potassium dichromate
KCl	Potassium chloride
min	Minute/or minutes
MI-Cl-FDU-12	1-methyl-3-(triethoxysilylpropyl) imidazolium chloride-functionalized FDU-12
mL	Milliliter/ or milliliters
M−TESP−IC	1-methyl-3 (triethoxysilylpropyl)imidazolium chloride
OMS	Ordered mesoporous silica
PP	Polypropylene
rpm	Revolutions per minute
SAMs	Silica-based adsorbent materials
S_{BET}	BET surface area
SCAs	Silane coupling agents
Si–$(OR)_4$	Tetralkylorthosilicate
TMB	1,3,5 trimethylbenzene
TPV	Total pore volume (cm^3 g^{-1})
TEM	Transmission electron microscopy

1. Introduction

In our modern life, the increasing contamination of water sources with toxic hexavalent chromium (Cr(VI)) poses a significant threat to human health and the environment. Cr(VI) is a highly toxic form of chromium with detrimental effects on humans, animals, and plants. It is reported that the toxicity of Cr(VI) is 100 times that of Cr(III) because Cr (VI) can easily penetrate biological membranes, induce oxidative stress, and lead to respiratory system damage, carcinogenesis, genotoxicity, immunotoxicity, and reproductive toxicity in humans [1]. Animals experience gastrointestinal distress, kidney and liver damage, hematological abnormalities, and neurotoxicity [2]. Plants suffer reduced growth, impaired photosynthesis, oxidative damage, nutrient uptake disruption, and death [3]. Hexavalent chromium generates reactive oxygen species, causes DNA damage, and is a known carcinogen, posing risks of lung, nasal, sinus, and gastrointestinal cancers. Its bioaccumulation potential disrupts ecosystems, necessitating monitoring, regulation, and effective remediation strategies for human, animal, and plant health protection.

The remediation of Cr(VI) from aqueous solutions has become a pressing concern, spurring the development of efficient and sustainable removal methods. Among various removal methods for toxic organic and inorganic species, the adsorption technique has attracted a tremendous deal of interest due to its simplicity in design, versatility, ease of working conditions, lack of sludge problem, low energy consumption, and variety in design [4–7]. Table 1 represents the general methods alongside their advantages and disadvantages for the removal of Cr(VI) from the water environment. Additionally, adsorbents can be easily regenerated and reused, further enhancing their sustainability and economic viability. In this context, the concept of eco-design has gained considerable importance, aiming to synthesize adsorbents using environmentally friendly approaches and utilizing cost-effective renewable resources [8–10]. Nevertheless, it is necessary to mention that although low-cost bio-based materials (such as microalga, bone waste, etc.) have been reported as adsorbents for pollutants such as heavy metals and dyes [11,12], the importance of high adsorption capacity, designability of the adsorbent, and ability to regenerate the adsorbent are of great importance. Designable biogenic adsorbents with nanostructures can be used to address this concern.

The emergence of nanomaterials and their nanocomposites has revolutionized various fields such as catalysis [13], tissue engineering [14,15], adsorption and extraction [16], etc. Nanomaterials possess

Table 1
Reported methods for Cr(VI) removal.

Treatments	Explanations	
Adsorption	Process details	Adsorbents like activated carbon, zeolites, or nanoparticles are used to adsorb Cr(VI) ions from water
	Advantages	High adsorption capacity, widely available adsorbents, relatively low cost, and can be regenerated and reused
	Disadvantages	Adsorbents may need regeneration, adsorption capacity can be influenced by water chemistry, and disposal of used adsorbents can be a concern
Chemical Reduction	Process details	Chemical reducing agents such as sodium bisulfite, ferrous sulfate, or sodium metabisulfite are added to water to convert Cr(VI) to less toxic Cr(III)
	Advantages	Simple and cost-effective method, widely applicable
	Disadvantages	May require pH adjustment, produces sludge or waste, and the effectiveness can be influenced by the presence of other water constituents
Ion Exchange	Process details	Ion exchange resins are used to exchange Cr(VI) ions with less harmful ions, such as chloride or sulfate
	Advantages	Efficient removal, selective for Cr(VI), can be regenerated and reused
	Disadvantages	Expensive initial setup and operation, disposal of spent resins can be an issue, and may require pretreatment for high fouling potential
Membrane Filtration	Process details	Reverse osmosis (RO) or nanofiltration (NF) membranes are used to separate Cr(VI) ions from water based on molecular size and charge
	Advantages	Effective removal, suitable for a wide range of water qualities, and can be combined with other treatment methods
	Disadvantages	High energy requirements, membrane fouling can occur, and higher capital and operational costs
Electrocoagulation	Process details	Applying an electric current to electrodes in water causes the formation of coagulants that bind to Cr(VI) ions, forming larger particles that can be easily separated
	Advantages	Effective for a wide range of water qualities, can remove other contaminants, and can be automated
	Disadvantages	Requires a power source, may generate additional sludge, and electrode maintenance is necessary
Biological Reduction	Process details	Microorganisms or microbial consortia are used to convert Cr(VI) to Cr(III) through biological reduction processes
	Advantages	Environmentally friendly, low energy consumption, can be effective at low Cr(VI) concentrations, and can be integrated into existing wastewater treatment systems
	Disadvantages	Slower treatment rates compared to some other methods, requires suitable microbial cultures, and can be influenced by pH, temperature, and nutrient availability
Precipitation	Process details	Chemicals such as calcium hydroxide, ferrous sulfate, or aluminum sulfate are added to water to precipitate Cr(VI) as insoluble compounds that can be easily separated
	Advantages	Relatively simple and cost-effective, effective at high Cr(VI) concentrations, and can be combined with other treatment processes
	Disadvantages	Requires proper pH adjustment and settling/filtration steps, can generate large volumes of sludge, and the presence of interfering substances can reduce efficiency
Photocatalysis	Process details	Semiconductor photocatalysts, such as titanium dioxide (TiO2), are used to generate reactive species that can oxidize or reduce Cr (VI) in the presence of light
	Advantages	Potential for complete mineralization of Cr(VI), can be effective under mild conditions, and can degrade other organic pollutants simultaneously
	Disadvantages	Limited by the availability of suitable photocatalysts, requires a light source, and may be influenced by water quality and the presence of competing substances
Constructed Wetlands	Process details	Wetland systems are designed to utilize natural processes and vegetation to remove contaminants, including Cr(VI), through adsorption, precipitation, and microbial activity
	Advantages	Sustainable and environmentally-friendly approach, long-term operation, cost-effective for large-scale applications, and can provide additional ecosystem benefits
	Disadvantages	Requires adequate space, longer treatment times, effectiveness can be influenced by climatic conditions, and may require pretreatment for high Cr(VI) concentrations
Biological Sorption	Process details	Living organisms, such as algae or macrophytes, are used to adsorb or accumulate Cr(VI) from water through sorption mechanisms
	Advantages	Natural and eco-friendly approach, can be integrated with existing biological systems, and potential for simultaneous nutrient removal
	Disadvantages	Limited capacity at high Cr(VI) concentrations, requires appropriate species selection, and potential release of Cr(VI) during biomass decay

unique properties such as high surface area and customizable surface properties, making them promising candidates for a broad range of applications. However, the field of adsorption, especially in the context of addressing environmental concerns, deserves more attention due to the urgent need for effective solutions to global environmental problems. The properties of nanomaterials and nanocomposites have been extensively investigated both experimentally and theoretically [17], contributing to a deep understanding of their behavior at the nanoscale. This combined approach has significantly enhanced our knowledge of nanomaterials and their potential applications in various fields.

SAMs have emerged as a compelling area of research in the field of removal technology. Among them, nanoporous SAMs have garnered considerable attention owing to their remarkable features and potential applications [18,19]. These materials exhibit remarkable features, including the ability to tailor their pore size, shape, particle morphology, particle size, and surface area, allowing for precise control and customization [20]. Additionally, their surfaces can be functionalized, enabling further versatility and adaptability for specific removal needs [19]. One of the key advantages of SAMs is the abundance of silica sources, making them readily available and economically viable. Moreover, these materials exhibit non-toxic characteristics, making them safer for both human health and the environment. Furthermore, the design flexibility of SAMs allows for the optimization of their performance, ensuring maximum effectiveness in specific removal scenarios. Researchers and engineers can fine-tune the material properties to address diverse challenges and tailor the adsorbents to meet specific requirements. The environmentally friendly nature of SAMs aligns with the growing demand for sustainable technologies that minimize adverse impacts on ecosystems.

Eco-design approaches in the synthesis of SAMs offer several advantages over traditional methods that use synthetic and commercially available silica sources such as $Si–(OR)_4$ and Na_2SiO_3 solution. Agricultural waste materials are abundant, renewable, and cost-effective, providing a sustainable alternative to conventional silica sources [21,22]. By utilizing sorghum waste, this study demonstrates the potential of integrating waste valorization and eco-design principles in the synthesis of adsorbent materials. This approach not only minimizes the ecological footprint but also fosters the advancement of a circular economy, wherein waste materials undergo a transformation into valuable resources. By utilizing renewable resources as starting materials, such as sorghum waste as a green silica source in this study, the environmental impact of the synthesis process is significantly reduced.

Moreover, the integration of green chemistry principles ensures the use of non-toxic reagents and solvents, minimizing potential hazards to human health and the ecosystem. The emphasis on eco-design aligns with the growing global focus on sustainable development and provides a pathway for the production of environmentally friendly adsorbents for water remediation applications. The utilization of agricultural waste, such as sorghum, as a silica source in the preparation of silica-based adsorbents holds great promise. Sorghum (sorghum bicolor [L.] Moench) is ranked as the fifth most significant cereal crop globally, following corn, wheat, rice, and barley according to FAO report [23,24]. According to the FAO report, the leading countries in sorghum production are the United States, which cultivates sorghum on 2.0 million hectares and yields an annual grain production of 8.7 million tons. Nigeria follows closely, with 6.9 million tons of sorghum produced on 5.4 million hectares. Ethiopia contributes 5.3 million tons from 1.9 million hectares, while Sudan produces 3.7 million tons on 6.8 million hectares. [23,24].

Among different types of nanoporous SAMs, OMS materials possess a well-defined pore structure with fixed pore diameter, pore volume, and high surface area, providing a large number of active sites for adsorption. The functionalizable surface of these materials allows for tailored modifications, enhancing their selectivity and adsorption capacity. Furthermore, mesoporous silicates exhibit excellent mechanical and chemical stability, ensuring their long-term performance in water treatment applications. Importantly, the non-toxic nature of the silica structure ensures that the adsorbents do not introduce additional contaminants into the water during the remediation process. FDU-12, as a member of the family of OMS materials, offers distinct advantages over other well-known family members such as SBA-15, SBA-16, KIT-5, KIT-6, MCM-41, MCM-48, etc. One of the notable advantages is its larger pore diameter, which provides enhanced accessibility and facilitates efficient diffusion of target contaminants into the mesoporous structure, enabling rapid and effective adsorption [25]. Moreover, FDU-12 exhibits a relatively thicker wall thickness compared to other mesoporous silicates. This characteristic contributes to its improved mechanical stability and resistance to collapse or structural damage during adsorption processes. The thicker walls enhance the robustness and durability of FDU-12, making it suitable for various environmental applications such as water remediation.

In the synthesis of functionalized-SAMs/and OMSs, the choice of preparation method plays a crucial role in determining the material properties and performance. Generally reported, there are two modification methods for the preparation of functionalized mesoporous silica, namely (1) one-pot co-condensation (or direct) synthesis and (2) post-synthesis (or grafting) [26]. One-pot synthesis method, such as the approach taken in this work to synthesize MI-Cl-FDU-12 using sorghum waste, offers several advantages over post-synthetic method. One-pot synthesis allows for the simultaneous incorporation of functional groups during the synthesis process, ensuring homogeneous distribution and improved accessibility of the active sites. This method also simplifies the synthesis procedure, reducing the number of steps and reaction times, and thereby enhancing the efficiency of adsorbent production.

In summary, this paper highlights the importance of eco-design in the synthesis of new adsorbent materials for the remediation of toxic hexavalent chromium. This paper investigates the synthesis and performance of a positively charged surface mesoporous silica FDU-12 anion-exchange adsorbent, namely MI-Cl-FDU-12, highlighting the significance of eco-design in the Cr(VI) removal and the synthesis of novel adsorbents. Adsorption emerges as a favorable method for Cr(VI) removal, offering advantages such as high efficiency, versatility, and ease of regeneration. SAMs, exemplified by the mesoporous FDU-12 material, exhibit exceptional properties, including large pore diameter, high surface area, and functionalizable surface, making them ideal for environmental applications. The one-pot synthesis method, employed to synthesize MI-Cl-FDU-12 using sorghum waste, showcases the advantages of this approach in terms of simplicity, efficiency, and homogeneous functional group distribution. The use of agricultural waste as a silica source further aligns with the principles of sustainability and waste valorization, contributing to the development of environmentally friendly adsorbent materials for water remediation applications.

2. Materials and methods

2.1. Chemicals

Triblock copolymer $EO_{106}PO_{70}EO_{106}$ (F127), $K_2Cr_2O_7$ (≥99.9%, MW: 294.19 g mol^{-1}), CPTES (95%, MW: 240.80 g mol^{-1}), 1-MI (99%, MW: 82.106 g mol^{-1}), and TMB (98%, MW: 120.19 g mol^{-1}) were purchased from Sigma-Aldrich (Germany). KCl (MW: 74.55 g mol^{-1}), NaOH (pellets, ≥97%, MW: 40.00 g mol^{-1}), and HCl fuming (37%) were purchased from Merck Millipore (Germany). Ethanol (96%v/v) were obtained from Dr. Mojallali Chemical Lab. (Tehran, Iran). In this work, DDW was utilized throughout the preparation procedure of the samples as well as heavy metal adsorption experiments.

2.2. Instruments and methods

For visual observation of the sample's morphology and pore structure, FESEM and TEM techniques were conducted using a MIRA3 TESCAN-XMU instrument (Kohoutovice, Czech Republic) and a Philips CM120 microscope (Eindhoven, Netherlands). The FESEM-mapping technique was used to determine the distribution of elements on the sample's surface.

The FTIR spectrum of the powdered sample, which was mixed with dried KBr, was recorded on an Avatar 370 instrument manufactured by Thermo Nicolet in the USA. The measurement was performed at room temperature, covering the spectral region from 4000 to 400 cm^{-1}.

Nitrogen adsorption–desorption isotherms were obtained at a temperature of 77 K using a BELSORP-mini II volumetric adsorption analyzer manufactured by BEL Japan Inc. in Osaka, Japan. The BET, *t*-plot, and 2D-NLDFT methods were used for estimating the surface area, microporous volume, and pore diameter, respectively.

The concentrations of Cr(VI) in aqueous solutions were determined using an ICP-OES model Optima 7300 DV manufactured by PerkinElmer Co. in the USA. The pH values of the solutions were adjusted using an Ohaus ST5000-F Benchtop pH Meter with Touchscreen.

Sonication was carried out using an SW3H ultrasonic cleaning apparatus manufactured by Sonoswiss AG in Ramsen, Switzerland, operating at a frequency of 37 kHz. Mechanical shaking of the bottles in adsorption tests was performed using a digital precise shaking water bath manufactured by Daihan Scientific Co. Ltd. in Korea. This equipment allowed for adjustment of time, temperature, and rotation per minute (rpm).

ChemBioDraw 20.0 software was utilized for drawing chemical molecules and structures. The graphical data were analyzed and visualized using Origin 8.6 software developed by Origin Lab Corporation in the USA. PSD (pore size distribution) calculations for N_2 adsorption were carried out using SAIEUS software provided by Micromeritics Instrument Corp., employing appropriate 2D-NLDFT models.

2.3. Preparation of Na_2SiO_3 solution from sorghum

Grass sorghum samples were procured from a local post-harvesting facility located in Rehann, Esfahan province, Iran. The samples were subjected to a thorough rinsing process employing tap water to eliminate extraneous particulate matter such as dust and sand. Subsequently, the sorghum underwent a prolonged period of desiccation in an electric oven maintained at a temperature of 363 K. The desiccated sorghum was then mechanically disintegrated into smaller particles, which were subsequently subjected to multiple cycles of DDW rinsing and

subsequent drying in an electric oven at 363 K for a duration of 12 h. To obtain silica particles of high purity, a mixture consisting of crushed sorghum (100 g) and HCl solution with a concentration of 0.1 N and a volume of 500 mL was introduced into a round-bottom flask with a capacity of 1000 mL. The mixture underwent rigorous agitation under reflux conditions for a period of 6 h at a temperature of 353 K, followed by ultrasonication for 30 min at 323 K. The resulting mixture was subsequently transferred to a stainless-steel autoclave reactor with a capacity of 1000 mL and maintained at a temperature of 393 K under a pressure of 15 lb per square inch (lbs) for a duration of 2 h. Finally, the acid-digested sorghum underwent repeated rinsing cycles with DDW to ensure complete removal of any residual HCl, followed by oven-drying at a temperature of 363 K. The sorghum was then placed in an electric muffle furnace and subjected to heating at a temperature of 873 K in the presence of an ambient air atmosphere for a duration of 2 h. By subjecting the resulting silica particles, characterized by a SiO_2 content of 93 %, to reflux conditions in a NaOH solution with a concentration of 2 mol L^{-1} in water at a temperature of 343 K for a duration of 24 h, a solution of Na_2SiO_3 was obtained.

2.4. One-pot synthesis of MI-Cl-FDU-12

The synthesis procedure of MI-Cl-FDU-12 is similar to a previous report regarding the synthesis of FDU-12 with some modifications [25]. MI-Cl-FDU-12 was prepared by direct synthesis method through co-condensation of Na_2SiO_3 and M−TESP−IC in the presence of F127 in an acidic solution medium. M−TESP−IC was synthesized by reactions between CPTES and 1-MI under nitrogen atmosphere according to the synthesis protocol reported by Soltani and co-workers in 2020 [27].

In a typical experimental procedure for MI-Cl-FDU-12, a quantity of 3.0 g of triblock copolymers $EO_{106}PO_{70}EO_{106}$ (F127, as templating agent), along with 3.0 g of TMB (as swelling agent) and 7.5 g of KCl (as additive), were dissolved in 180 mL of 2 mol L^{-1} HCl (as solvent/hydrolyzing agent) and subjected to stirring for a duration of 24 h. Subsequently, certain amounts of Na_2SiO_3 (as silica source) and M−TESP−IC (as functionalization agent, SCA) were introduced into the resulting reaction mixture, which was allowed to undergo further stirring for an additional 24 h at a temperature of 313 K. The mixture was then transferred to an autoclave and subjected to heating at the desired temperature for a period of 72 h. The solid product obtained was collected by means of filtration and subsequently dried at room temperature under atmospheric conditions. The resulting fine white powder was then introduced into a round-bottom flask containing a solution of HCl and ethanol, and the mixture was subjected to refluxing with continuous stirring while exposed to air overnight. Eventually, the resulting mixture was filtered using a Buchner funnel, washed three times with DDW and ethanol, and then dried in an oven at a temperature of 333 K for a duration of one day. The purified MI-Cl-FDU-12 material was stored in a glass bottle with a screw cap.

2.5. Adsorption tests

The stock solution of 1000 mg L^{-1} Cr(VI) was prepared in DDW using $K_2Cr_2O_7$. Working standards were prepared by diluting the stock solution with DDW every day. To investigate the effect of pH and adsorbent dose (W) on the adsorption process, three different doses of the adsorbent (1.0, 2.0, and 3.0 mg) were added in PP bottles containing a certain initial concentration (C_i=10 mg L^{-1}) of Cr(VI) solution at different pH range between 2.0 and 7.0. The solutions were then mechanically shaked at 298 K and 180 rpm for 40 min. Then the solutions were passed through Whatman 42 filter papers and the solutions and the filtrates were analyzed by ICP-OES in order to determine the concentration of the remaining total chromium ions. The same methodology was used for the kinetic and isotherm tests, with the exception that in the isotherm tests, the temperatures (T=298, 303, 308, and 313 K) and solution initial concentrations, C_i=1, 2, 3, 5, 10, 20, 50, 100, and 200 mg L^{-1}. Other experimental parameters where t=40 min, pH=3.0, dose=3.0 mg, V=25 mL, and agitation speed (180 rpm) were fixed. C_i for the kinetic study was 50 mg L^{-1} and samples were taken at time intervals (t=1, 2, 3, 4, 5, 10, 15, 20, 25, 30, and 40 min). All experiments were conducted in triplicate, and the outcomes were presented following the computation of the mean values.

All equations used for adsorption studies in this work are given in Table 2.

Table 2
Adsorption equations and different theoretical models used in this study.

Name/Model	Equations
General equilibrium aquations	
(1) Removal percentage (%)	$Removal = (C_i - C_e) \bullet (100/C_i)$
(2) Adsorption capacity at time t	$Q_t = (C_i - C_t) \bullet (W/V)$
(3) Adsorption capacity at equilibrium	$Q_e = (C_i - C_e) \bullet (W/V)$
Isotherm Models	
(4) Langmuir	$Q_e = (Q_{m,cal.} \bullet K_L \bullet C_e)/(1 + K_L \bullet C_e)$
(5) Freundlich	$Q_e = (K_F \bullet C_e^{1/n})$
(6) Temkin	$Q_e = (R \bullet T/b_T) \bullet \ln(K_T \bullet C_e)$
Kinetic Models	
(7) PFO	$Q_t = Q_{e,cal.} \bullet (1 - e^{-k_1 \bullet t})$
(8) PSO	$Q_t = (Q_{e,cal.}^2 k_2 \bullet t)/(1 + Q_{e,cal.} k_2 \bullet t)$
(9) Elovich	$Q_t = (1/\beta) \bullet \ln(\alpha \bullet \beta) \bullet t$
(10) Avrami	$Q_t = Q_{e,cal.} \bullet (1 - e^{(-k_{Av} \bullet t)^{n_{Av}}})$

3. Results and discussion

3.1. Synthesis procedure

A well-ordered mesostructured material with face-centered cubic structure ($Fm\bar{3}m$) symmetry designated as MI-Cl-FDU-12 can be synthesized using a straightforward, one-pot, and environmentally friendly hydrothermal approach. This method employs Na_2SiO_3 extracted from sorghum as a source of biogenic silica, triblock copolymer F127 ($EO_{106}PO_{70}EO_{106}$: PO is polypropylene oxide and EO is polyethylene oxide) as a template, TMB as a micelle expander or swelling agent, M−TESP−IC as a SCA or surface functionalization agent, KCl inorganic salt as an additive, HCl as a hydrolyzing agent, and water as a solvent. In the context of synthesizing mesoporous silica nanostructures, the one-pot co-condensation mechanism represents a notable strategy involving the simultaneous presence of an organic template, a SCA, and a silica source within the same aqueous solution, yielding advantageous outcomes. Specifically, the organic template, upon being dissolved in the solution, assumes a pivotal role in the generation of a mesoporous structure by providing a template or framework that determines the desired pore architecture. Concomitantly, the SCA and silica source experience hydrolysis within the aqueous milieu surrounding the organic template. The hydrolytic reaction entails the cleavage of chemical bonds present in the SCA and silica source molecules, facilitated by the presence of water. Subsequently, the hydrolyzed silane coupling agent and silica source undergo condensation reactions, leading to the formation of siloxane bonds, which act as linkages between the hydrolyzed species. Consequently, a cohesive silica network materializes. During the hydrolysis and condensation processes, the organic template orchestrates the assembly of the silica species, exerting influence over the ensuing mesoporous structure formation.

The template molecules serve as a scaffold around which the silica species organize themselves, thereby engendering the creation of mesopores with uniformity. The one-pot co-condensation mechanism bestows several merits, including its simplicity, diminished synthesis duration, and the ability to achieve precise control over the resultant mesoporous structure. As such, it emerges as a versatile and valuable approach for synthesizing OMS materials, with a broad range of applications spanning diverse domains such as adsorption, catalysis, drug delivery, and nanotechnology.

It has been observed that the leaf sheath epidermis of sorghum contains approximately 12 % ash and 88 % silica, making it an abundant and viable source of biogenic silica [28,29]. Accordingly, sorghum was selected as a potential alternative source of nanosilica to prepare an ordered mesoporous silica. The utilization of sodium silicate extracted from sorghum waste as a green silica source demonstrates the innovative use of sustainable materials in the synthesis process of silica-based nanomaterials.

Unlike the post-grafting functionalization method, where a silane coupling agent is added after the preparation of nanoporous silica and

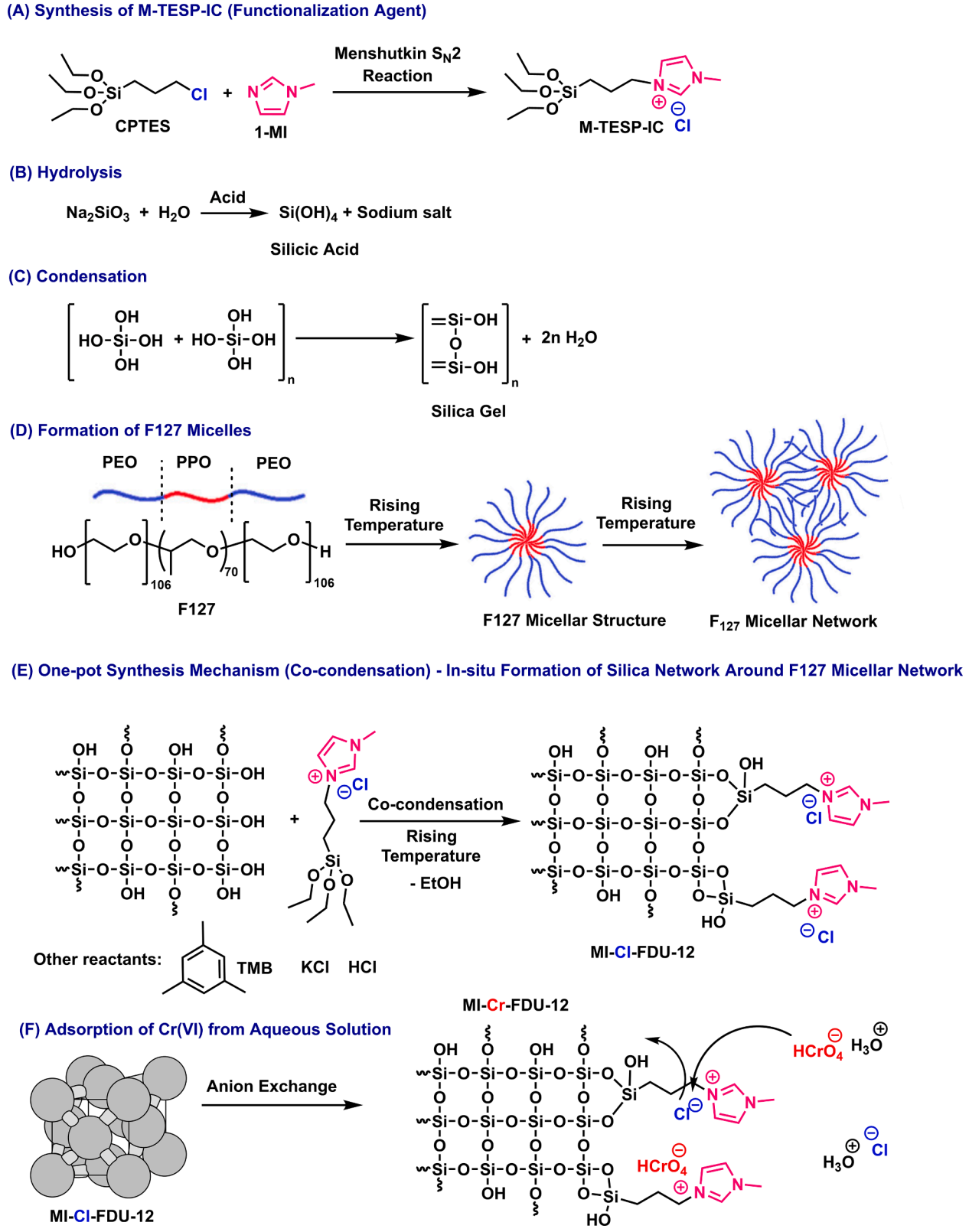

Scheme 1. Schematic representation for preparation of MI-Cl-FDU-12 anion exchange adsorbent for removal of hexavalent chromium oxyanions.

the removal of the surfactant template, the one-pot synthesis method requires the addition of the functionalization agent prior to template removal and during the addition of the silica source. This is necessary to ensure the preservation of the functionalization agent's integrity during the modified nanoporous silica preparation through one-pot synthesis protocol, as the organic moiety of silane coupling agents degrades when using the combustion surfactant removal method. To address this issue, an acid extraction method is employed to remove the organic template from the silica-surfactant composite precipitates while safeguarding the organic tail of the silane coupling agent. This approach offers two additional advantages over the post-grafting method using the combustion surfactant removal method: a shorter preparation time for functionalized nanosilica and the elimination of the furnace combustion stage, resulting in reduced electricity costs. It is reported that TMB is used as swelling agent to enlarge the entrance and cavity size in FDU-12 [30].

Additionally, it can infiltrate the hydrophobic region of organic micelles, thereby augmenting the proportion of the hydrophobic core and inducing a transition from the body-centered cubic arrangement ($Im\bar{3}m$) to a denser configuration ($Fm\bar{3}m$) [31].

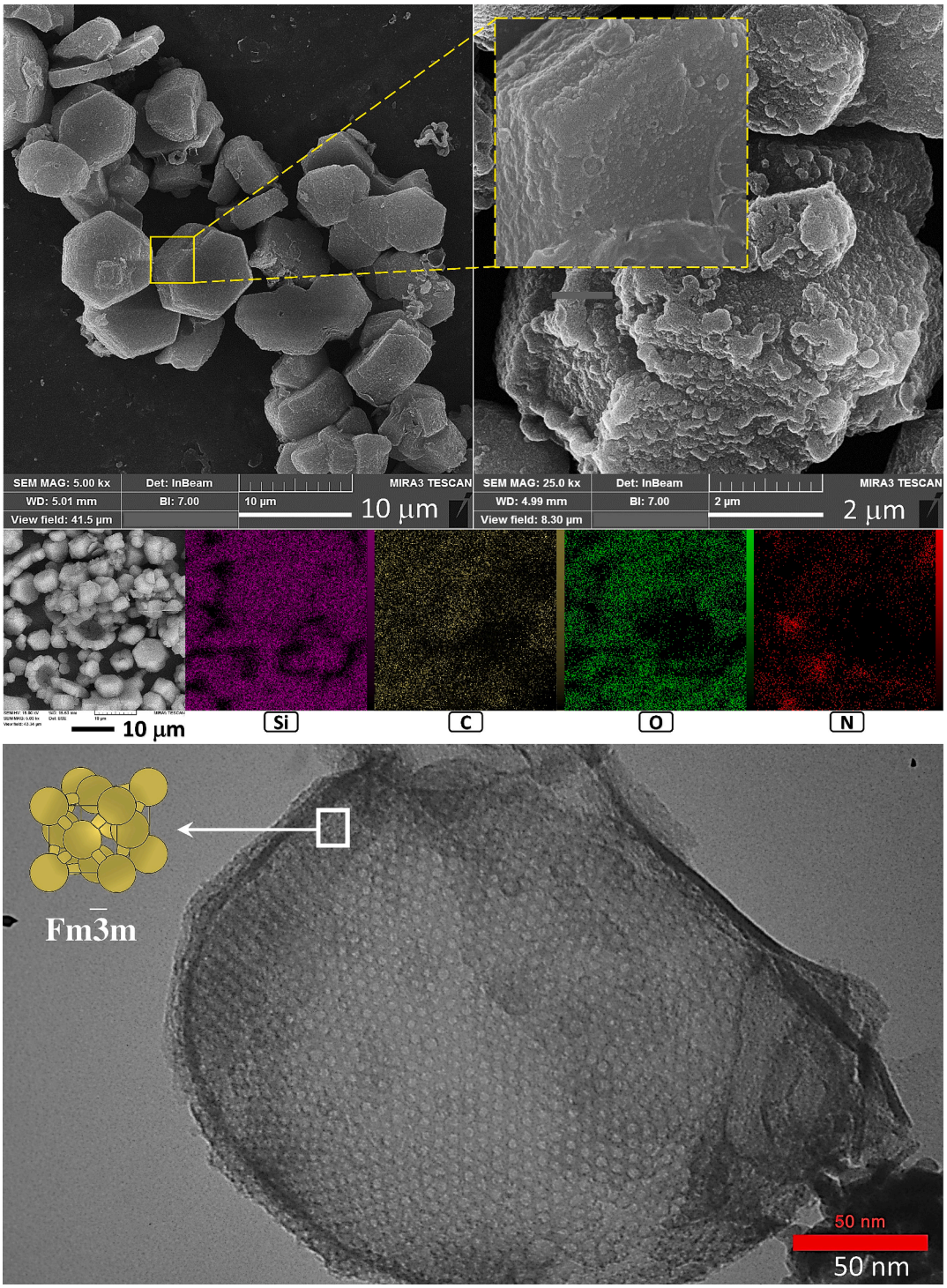

Fig. 1. FESEM images (first row), FESEM-Mapping images (second row), and TEM image of MI-Cl-FDU-12 (third row).

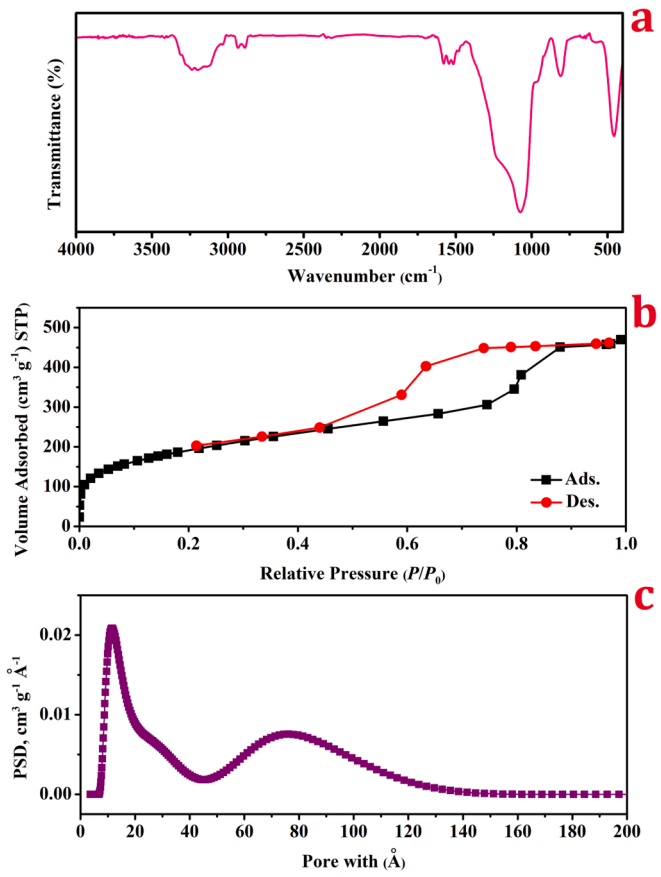

Fig. 2. FTIR spectrum (a), N_2 adsorption–desorption isotherms (b), and PSD diagram using 2D-NLDFT model (c).

The reason for choosing M−TESP−IC as SCA is its excellent ability to anion exchange in aqueous media. During the adsorption process, chlorine anions adjacent to methyl imidazolium can be easily exchanged with chromium anions in a anion exchange process. A schematic representation for preparation of MI-Cl-FDU-12 anion exchange adsorbent for removal of hexavalent chromium oxyanions is illustrated in Scheme 1.

3.2. Structure characterization of MI-Cl-FDU-12

FESEM and TEM analyzes were carried out to investigate the morphology of the adsorbent and its porous structure. As show in Fig. 1 (first row, picture on the right), the FESEM image with a magnification of 5000 (5.00 kx) clearly shows the regular hexagonal prism morphology, which indicates the high degree of purity of the synthesized material. The distribution of structural elements is also shown in Fig. 1 (second row) indicating a homogeneous distribution of Si, O, C, and N on the surface of MI-Cl-FDU-12. The origin of N located on the surface of the synthesized material is nitrogen used in the imidazole ring of M−TESP−IC which is indicative of successful incorporation of SCA in the structure of anion-exchanger adsorbent. Also, the origin of Si and O is related to the Na_2SiO_3 extracted from sorghum. Most of the origin of C is related to the organic moiety of the SCA, and part of it can also be considered related to the remaining organic template and the swelling agent remaining in the adsorbent structure. The TEM image shown in the third row of Fig. 1 clearly shows uniform *meso*-sized pores in the adsorbent structure. These pores have a space group $Fm\bar{3}m$ with a face-centered cubic structure [25]. The TEM images provide a clear demonstration of the molecular sieve structure of MI-Cl-FDU-12, which is characteristic of well-defined OMS materials.

To characterize the organic and inorganic functional groups of MI-Cl-FDU-12, FTIR spectrum of the sample was collected and shown in Fig. 2**a**. The appearance of characteristic absorption bands related to the vibrational modes at wavenumber (cm^{-1}) of 468 (Si-O-Si bending), 800 (Si-OH bending, symmetric), 1000–1100 (Si-O-Si stretching, symmetric), 1050–1200 (Si-O-Si stretching, asymmetric), 1550 (C═N stretching, imidazolium ring), 1580 (C═C stretching, imidazolium ring), 1600 (H—O—H bending, surface adsorbed water), 2850–2900 (C—H stretching, propyl chain of SCA and remaining F127 chain), 3000–3100 (C—H stretching, imidazolium ring), and 3250–3600 (Si-OH stretching) clearly demonstrated the successful formation of organic/inorganic hybrid structure of the MI-Cl-FDU-12 anion-exchanger adsorbent.

The N_2 adsorption–desorption isotherms of MI-Cl-FDU-12 is shown in Fig. 2**b**. The surface area of 672 $m^2\ g^{-1}$ and a total pore volume (TPV) of 0.725 $cm^3\ g^{-1}$ were calculated according to the BET model. The isotherms display a type IV shape, which is indicative of mesoporous structures with well-defined pore networks. The presence of a steep capillary condensation step suggests a uniform pore diameter within the material (larger cage-like mesopores), while the sharp capillary evaporation step at the lower end of the hysteresis loop indicates narrow pore entrances (window size). This observation aligns with the information obtained from the 2D-NLDFT PSD analysis (Fig. 2**c**), which identified two main pore size distributions at 1.2 nm (window size or entrance size) and 7.5 nm (pore size or cavity size). The decrease in pore size compared to previous reports (Table 3) is attributed to the incorporation of organic moieties inside the pores, leading to a natural reduction in pore size. However, the surface area and total pore volume of MI-Cl-FDU-12 are comparable to other FDU-12 samples reported in Table 3. The N_2 adsorption–desorption isotherm of MI-Cl-FDU-12 demonstrates its well-defined pore structure decorated with 1-MI functional groups, a high surface area, uniformity, and the presence of distinct pore sizes, highlighting its potential for applications requiring controlled porosity, high surface area, and functionality.

3.3. Adsorption studies

To assess the adsorption performance of the adsorbent, a series of systematic adsorption experiments were conducted. These tests examined the influence of various parameters, namely pH, adsorbent dose

Table 3
Comparison between textural and structural features of MI-FDU-12 in this work and those for previously reported ordered mesoporous silica FDU-12.

Name	S_{BET} ($m^2\ g^{-1}$)	Window size (nm)	Cavity diameter (nm)	TPV ($cm^3\ g^{-1}$)	Ref.
MI-FDU-12	672	1.2	7.5	0.72	This work
FDU-12–0	716	2.5	10.1	0.68	[32]
FDU-12–373	712	≈4	10.0	0.66	[25]
FDU-12–393	569	5.3	11.0	0.73	[25]
FDU-12–403	480	7.5	12.4	0.86	[25]
FDU-12–100	899	3.9	6.0	0.73	[33]
FDU-12–120	593	6.3	11.6	0.93	[33]
FDU-12–120-NH_2	326	6.1	10.2	0.63	[33]
L-FDU-12–100	610	<5	23.7	0.73	[34]
R-FDU-12–100	496	<5	16.7	0.69	[34]

(W, mg), solution temperature (T, K), initial concentration of the adsorbate (C_i, mg g^{-1}), and contact time (t, min). Additionally, the reusability of the adsorbent was investigated by monitoring its performance across multiple consecutive adsorption cycles. To gain insight into the underlying adsorption mechanism, several nonlinear isotherm models, including Langmuir [35,36], Freundlich [37], and Temkin [38,39], as well as kinetic models such as PFO [40], PSO [41], Elovich [42], and Avrami [43], were employed (as corresponding equations are given in Table 2). These models were fitted to the corresponding experimental data, and their parameters were compared and analyzed to determine the most suitable adsorption mechanism.

3.3.1. The effect of pH and adsorbent dose

Fig. 3 illustrates the combined influence of pH and adsorbent dose on the adsorption of Cr(VI). It is evident that the highest uptake of Cr(VI) occurs at pH 2.0 and 3.0, irrespective of the adsorbent dose. However, as the pH increases, there is a continuous decline in the removal efficiency. Concurrently, an increase in the dose from 1.0 mg to 3.0 mg resulted in an augmentation of the removal percentage across all pH values. Previous studies have reported that employing a higher dose leads to a greater observed removal efficiency. This can be attributed to the fact that an increased dose, under constant adsorbate volume and concentration, enhances the number of active adsorption sites, subsequently promoting the adsorption of the adsorbate. Under constant conditions, the optimal pH of 3.0 and a dose of 3.0 mg resulted in the maximum removal efficiency of 100 %. Consequently, pH 3.0 and a dose of 3.0 mg were selected as the optimal parameters for the subsequent stages of the adsorption tests.

In acidic environments, chromium exhibits the capability to generate several stable anionic species, whose stability and prevalence are contingent upon the specific pH range. For instance, CrO_4^{2-} demonstrate stability within moderately acidic to mildly alkaline conditions, predominantly manifesting in solutions with pH levels ranging approximately from 5.0 to 9.0. These $CrO4^{2-}$ oxyanions are characterized by their distinctive yellow tone. Conversely, under more acidic circumstances, the CrO_4^{2-} oxyanion has the potential to undergo protonation, resulting in the formation of $HCrO_4^-$ oxyanions. These $HCrO_4^-$ oxyanions exhibit stability at lower pH levels, generally within the pH range of 2.0 to 6.0, and are discernible by their orange coloration. Lastly, $Cr_2O_7^{2-}$ oxyanions endure in highly acidic conditions, specifically in solutions with pH values below 2.0, and are notably prevalent within strongly acidic environments [44]. $Cr_2O_7^{2-}$ ions are visually striking with their clear orange appearance. Considering this information and the experimental conditions observed in the pH test, the dominant chromium species adsorbed by the MI-Cl-FDU-12 adsorbent at pH 3.0 is $HCrO_4^-$.

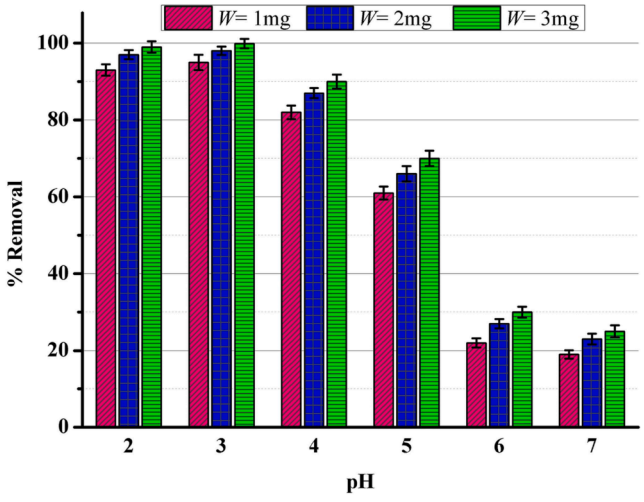

Fig. 3. The combined influence of pH and adsorbent dose on the adsorption of $HCrO_4^-$ under constant condition (C_i=10 mg L^{-1}, V=25 mL, W=3.0 mg, T=298 K, t=40 min, agitation speed=180 rpm).

At this pH, the positively charged surface of MI-Cl-FDU-12 exhibits a strong electrostatic attraction towards these $HCrO_4^-$ oxyanions. This electrostatic interaction facilitates an anion exchange process, wherein the $HCrO_4^-$ anion interacts with adjacent chlorine anions placed to the positively charged methyl imidazolium ring of the adsorbent. As a result of this exchange, the chlorine anions are released into the solution. The anion exchange mechanism observed in this system is consistent with the principles of ion exchange, a well-established phenomenon in chemistry. Anion exchange involves the reversible exchange of anions between a solid phase and a liquid phase, driven by the difference in affinity between the exchanged ions and the solid surface. In the case of MI-Cl-FDU-12, the positively charged surface attracts and exchanges $HCrO_4^-$ anions with chlorine anions, leading to the liberation of chlorine into the surrounding solution. This anion exchange process facilitated by MI-Cl-FDU-12 demonstrates the material's ability to effectively capture and remove $HCrO_4^-$ species from aqueous solutions under acidic conditions. It highlights the significance of surface charge interactions and ion exchange phenomena in the adsorption mechanism, providing insights into the underlying mechanisms governing the adsorption behavior of MI-Cl-FDU-12 as a potential Cr(VI) anion exchanger adsorbent.

3.3.2. The effect of initial concentration and temperature and isotherm studies

The graph in Fig. 4**a** presents the variation in the percentages of $HCrO_4^-$ removal in relation to the corresponding C_i. It is evident that as the C_i increases from 1 to 200 mg L^{-1}, the removal efficiency steadily decreases. However, for removal percentages, the rate of decrease in the C_i range of 1 to 50 mg L^{-1} is lower than that beyond this range (50 to 200 mg L^{-1}). Additionally, it was observed that higher temperatures result in increased removal efficiency at all initial concentrations. Consequently, elevated temperatures have a positive influence on the removal performance of $HCrO_4^-$ by MI-Cl-FDU-12 anion exchanger. For initial concentrations below 50 mg L^{-1} and across all temperatures, removal percentages exceeding 80 % were observed. Therefore, it can be concluded that MI-Cl-FDU-12 demonstrates favorable adsorption performance for $HCrO_4^-$ oxyanions with C_i values up to 50 mg L^{-1} within a temperature range of 298 to 313 K in aqueous solutions.

To investigate the potential mechanism involved in the adsorption of $HCrO_4^-$ oxyanions by the adsorbent, the adsorption capacities corresponding to equilibrium concentrations need to be calculated. Fig. 4**b** depicts the relationship between changes in Q_e and the corresponding C_e values. Nonlinear versions of three two-parameter isotherm models, namely Langmuir, Freundlich, and Temkin, were applied to fit the experimental data at four different temperatures, and their fitted diagrams are displayed in Fig. 4**c-f**. It is acknowledged that nonlinear equations provide more precise data compared to their linear counterparts, because the linearization process alters the relationship between independent and dependent variables [44]. This procedure can introduce errors to both the independent and dependent variables and may lead to inaccurate parameter estimations. To obtain consistent and accurate parameter estimations, a nonlinear method is recommended [45,46].

The obtained isotherm data following the analysis of nonlinear fitting are presented in Table 4. The analysis of the obtained data indicates that the Langmuir model exhibits the closest agreement with the experimental data at three temperatures among the isotherm models considered, as determined by the R^2_{Adj} values. Specifically, the trend observed for the best-fitted model based on the R^2_{Adj} values if Langmuir > Temkin > Freundlich models. Furthermore, the close agreement between $Q_{m,cal.}$ values predicted by the Langmuir model and $Q_{m,exp.}$ values across all temperatures indicates the Langmuir model's strong fit to the experimental data on $HCrO_4^-$ adsorption by the anion exchanger

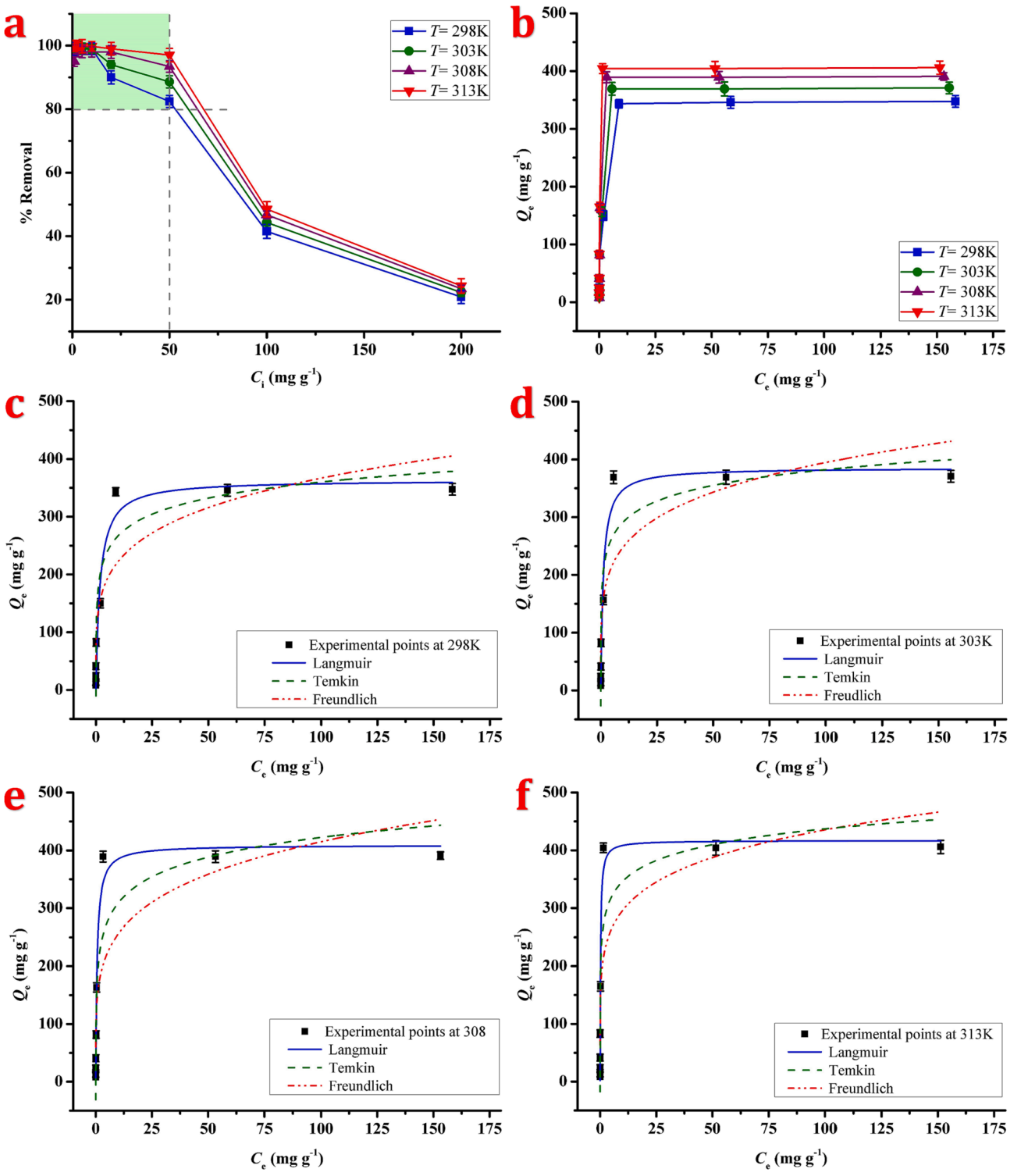

Fig. 4. The combined influence of initial concentration of Cr(VI) (C_i=1 to 200 mg L^{-1}) and temperature (T=298, 303, 308, and 313 K) on the removal efficiency of $HCrO_4$ under constant condition (pH=3.0, W=3.0 mg, V=25 mL, t=40 min, agitation speed=180 rpm) (a). Q_e changes *vs* corresponding C_e values at differetn temperatures (b). Isotherm models fitted to the experimental points at 298 K (c), 303 K (d), 308 K (e), and 313 K (f).

adsorbent. The calculated values of $Q_{m,cal.}$ at temperatures 298 K, 303 K, 308 K, and 312 K are 363.5 mg g^{-1}, 385.5 mg g^{-1}, 409.0 mg g^{-1}, and 416.9 mg g^{-1}, respectively. These results demonstrate a positive correlation between temperature and the adsorption capacity of $HCrO_4^-$ within the temperature range of 298 K to 313 K. According to the Langmuir model, the rates of adsorption and desorption on the surface are equal. Additionally, based on the assumptions of the Langmuir model, the adsorbed layer in the case of $HCrO_4^-$ adsorption consists of a single molecule (monolayer adsorption) occurring at specific localized sites. There is no steric hindrance or lateral interaction between adjacent adsorbed molecules. Moreover, the adsorption is characterized by homogeneity, with each molecule possessing sorption activation energy and constant enthalpies. All sites exhibit equal affinity for the adsorbate, and there is no transmigration of adsorbate in the surface plane.

Table 4
The values of isotherm models' parameters at different temperatures.

	T	298 K	303 K	308 K	313 K
	$Q_{m,exp.}$	347.5	370.8	390.8	405.2
Langmuir	$Q_{m,cal.}$	363.5	385.5	409.0	416.9
	K_L	0.549	0.911	1.596	4.721
	$R^2_{Adj.}$	0.9432	0.9561	0.9822	0.9726
Freundlich	n	4.626	4.969	4.766	5.964
	$1/n$	0.216	0.201	0.210	0.168
	K_F	135.5	156.2	157.8	201.1
	$R^2_{Adj.}$	0.8416	0.8249	0.7343	0.7684
Temkin	b_T	0.024	0.026	0.020	0.025
	K_T	77.25	170.1	53.27	643.9
	$R^2_{Adj.}$	0.9322	0.9052	0.8646	0.8949

The Temkin isotherm model exhibits a linear decline in the heat of adsorption ($\Delta H_{ads.}$) for all molecules within the adsorption layer, owing to the interactions between the adsorbent and the adsorbate. Another noteworthy characteristic of the Temkin model is its consideration of a homogeneous distribution of binding energies across all adsorption sites, while disregarding extremely high and low concentration values [47,48]. Consequently, this model is solely applicable within an intermediate concentration range. In the present study, the Temkin model demonstrates the exothermic nature of adsorption, as indicated by a positive value of parameter b_T, which signifies the release of heat during the process.

In the Freundlich model, the isotherm type is determined by the value of temperature-dependent n parameter. The value of $1/n$ represents the surface heterogeneity or the intensity of adsorption. When $1/n$ is between zero and unity ($0<1/n<1$), the adsorption process is considered favorable. When $1/n$ is greater than 1 ($1<1/n$), the adsorption process is unfavorable, and when $1/n$ equals 1, it is irreversible ($1/n=1$). In Table 4, the $1/n$ values for the adsorption of $HCrO_4^-$ on the adsorbent range from 0.168 to 0.216, indicating a favorable adsorption process.

3.3.3. *The effect of contact time and kinetic studies*

The assessment of adsorbent efficiency for practical applications necessitates the consideration of adsorption time as a crucial determinant. A reduced adsorption time enhances the affordability and operational efficiency of the adsorbent. To this end, alterations in the adsorption capacity of the adsorbent were examined over time, and the outcomes are presented in Fig. 5a (where solid squares denote the experimental data points). Following an initial 5-minute adsorption period, a rapid adsorption gradient was observed, succeeded by a gradual adsorption gradient until reaching the equilibrium point and attaining adsorbent saturation within 30 min. No significant alterations were observed beyond the 30-min mark. Thus, the optimal adsorption time for $HCrO_4^-$ oxyanions by the adsorbent was determined to be 30 min.

To investigate the adsorption kinetics involved in $HCrO_4^-$ ion removal by the adsorbent, four distinct kinetic models were employed. Subsequently, the obtained parameters of these nonlinear models were fitted to the experimental data and compared with one another. The calculated kinetic data after nonlinear fitting are given in Table 5. Among the four models used, the Avrami model exhibited the best agreement with the experimental data based on $R^2_{Adj.}$ values, followed by the PFO, PSO, and Elovich models. However, in selecting the most suitable model, the proximity of the experimental adsorption capacity ($Q_{e,exp.}$) to the theoretical ($Q_{e,cal.}$) values should be considered, in addition to the comparison of $R^2_{Adj.}$ values. Comparing the $Q_{e,cal.}$ values and $Q_{e,exp.}$ (=343.3 mg g^{-1}) value, it is noted that the order of preference is PFO (=341.9 mg g^{-1}) > Avrami (=331.1 mg g^{-1}) > PSO (=403.0 mg g^{-1}).

The PFO and PSO kinetic models effectively describe the correlation between the adsorbate in the solution and the occupation of the functional groups, also known as adsorbent active sites, involved in the adsorption process. Specifically, the PFO model accurately represents a limited number of surface-active site occupations, while the PSO model provides a depiction of a larger proportion of these occupations. However, it should be noted that in actual adsorption processes, the

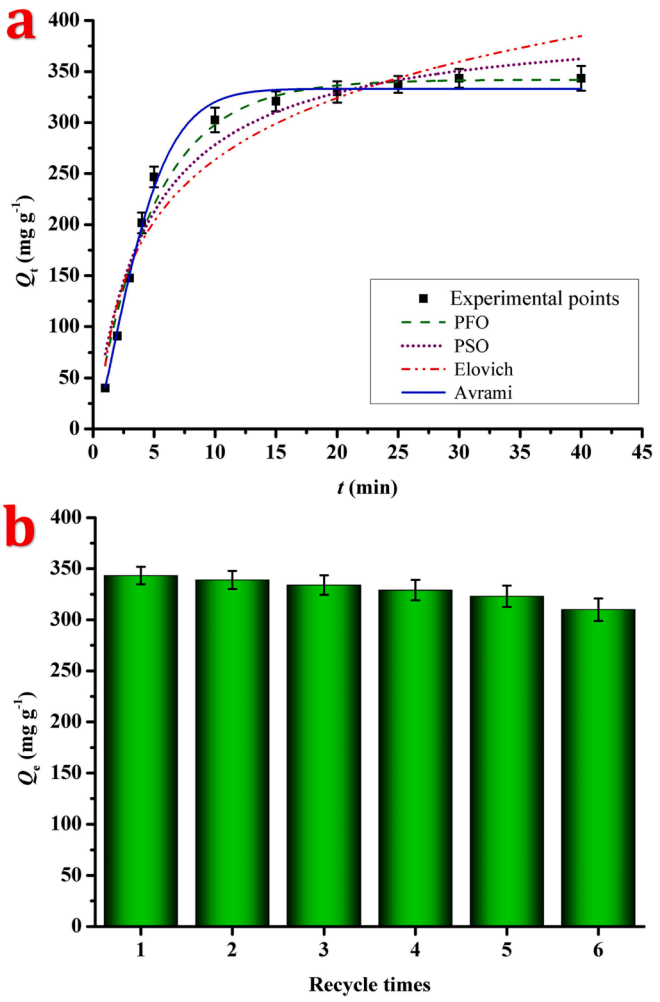

Fig. 5. The influence of contact time (t=1, 2, 3, 4, 5, 10, 15, 20, 25, 30, 40 min) on adsorption capacity of $HCrO_4^-$ under constant conditions (pH=3.0, W=3.0 mg, V=25 mL, C_i=50 mg L^{-1}, agitation speed=180 rpm) and nonlinear kinetic models fitted to them (a). Q_e changes *vs* number of recycle time under constant conditions (pH=3.0, W=3.0 mg, V=25 mL, C_i=50 mg L^{-1}, t=40 min, agitation speed=180 rpm) (b).

Table 5
The values of kinetic models' parameters at 298 K.

Models	**Parameters**	**Values**
	$Q_{e,exp.}$	343.3
PFO	$Q_{e,cal.}$	341.9
	k_1	0.205
	$R^2_{Adj.}$	0.9801
PSO	$Q_{e,cal.}$	403.0
	k_2	5.533
	$R^2_{Adj.}$	0.9553
Elovich	α	177.9
	β	0.011
	$R^2_{Adj.}$	0.9274
Avrami	$Q_{e,cal.}$	331.1
	$k_{Av.}$	0.232
	$n_{Av.}$	1.394
	$R^2_{Adj.}$	0.9913

occupations of the adsorbent active sites exhibit a higher level of complexity. For instance, during the initial stage of adsorption, only a few active sites are occupied, and this phenomenon can be effectively captured by the PFO model. Conversely, during the final stage of adsorption, a majority of the active sites become occupied, and the PSO model may offer a superior description of this process. Consequently, the PFO and PSO models exclusively address specific conditions within the adsorption process and do not encompass its entirety.

The Avrami kinetic model is applicable in scenarios involving multiple adsorption mechanisms and postulates that the adsorption mechanism can follow multiple kinetic orders that undergo changes throughout the interaction between the adsorbate and the adsorbent [49,50]. Accordingly, in this particular study, the kinetics of adsorption of the $HCrO_4^-$ oxyanion can be described as a combination of the PFO and PSO models. During the initial stage, when the adsorption process is characterized by a rapid rate, the PFO model provides an accurate prediction of the adsorption behavior. Subsequently, as the rate of adsorption diminishes, the PSO model offers a better depiction of the adsorption behavior. Nevertheless, it is worth noting that the $Q_{e,exp.}$ value and $Q_{e,cal.}$ value obtained from the PFO model exhibit closer agreement, suggesting that the PFO model slightly outperforms the PSO model in terms of predicting the adsorption behavior.

3.3.4. Reusability performance of the adsorbent

The evaluation of an adsorbent's suitability for real-world applications and large-scale usage critically hinges on its reusability, necessitating stability during recovery and the ability to be reused and regenerated after multiple successive uses. To adhere to established guidelines from prior study regarding the selection of an appropriate desorption eluent for Cr(VI) [27], a 0.1 mol L^{-1} NaOH solution was employed. Following a 40-min exposure to an aqueous Cr(VI) solution, the MI-Cl-FDU-12 anion exchanger was subjected to subsequent cycles of Cr(VI) adsorption, with regeneration accomplished using 25 mL of 0.1 mol L^{-1} NaOH. The regenerated anion exchange adsorbent thus obtained was employed for successive adsorption of Cr(VI) under optimal experimental conditions, encompassing six consecutive adsorption–desorption cycles. It is noteworthy that the adsorbent surface was cleansed of unwanted ions by employing DDW water after each adsorption/desorption cycle.

The Cr(VI) adsorption capacity of the adsorbent, as it underwent the six cycles, is illustrated in Fig. 5b. The observed constancy in the Cr(VI) adsorption capacity of MI-Cl-FDU-12 throughout the six cycles suggests the absence of irreversible adsorption sites on the surface of the anion exchange adsorbent. Thus, the MI-Cl-FDU-12 anion exchanger exhibits favorable recyclability. The regeneration of the adsorbent through treatment with NaOH implies that the adsorption of Cr(VI) by the adsorbent occurs *via* reversible anion exchange processes and electrostatic interactions. Furthermore, the reduction in adsorption capacity of the reused adsorbent (from about 343 mg g^{-1} in the first cycle to about 305 mg g^{-1} in the sixth cycle) can plausibly be attributed to the gradual loss of adsorbent mass over the course of the six consecutive adsorption–desorption cycles.

3.3.5. Comparison study

Table 6 provides a comprehensive comparative analysis of recently reported adsorbents for Cr(VI), along with the corresponding optimal parameters. The data presented in Table 6 unveils noteworthy findings regarding the performance of various adsorbents in relation to Cr(VI) adsorption. Among these adsorbents, MI-CL-FDU-12 stands out as an exceptional candidate, exhibiting an outstanding adsorption capacity that surpasses that of most previously reported Cr(VI) adsorbents. Specifically, the adsorption capacity of MI-CL-FDU-12 at 298, 303, 308, and 313 K found to be 363.5, 385.5, 409.0, and 416.9 mg g^{-1}, respectively. Moreover, MI-CL-FDU-12 demonstrates a remarkably shorter adsorption time in comparison to the majority of adsorbents listed in Table 6. The adsorption time for MI-CL-FDU-12 was measured to be 40 min, whereas the average adsorption time reported for other adsorbents was between 1 and 24 h. This shorter adsorption time indicates the rapid kinetics of the MI-CL-FDU-12 adsorbent, suggesting its potential applicability in real-world scenarios where time efficiency is crucial. The impressive adsorption performance and fast kinetics exhibited by MI-CL-FDU-12 make it a promising candidate for practical applications in Cr(VI) removal. These results highlight the significance of MI-CL-FDU-12 as a highly effective and efficient adsorbent, paving the way for its potential utilization in various industries and environmental remediation processes.

Table 6
The comparison table regarding adsorption capacity of Cr(VI) of several adsorbents under optimal conditions.

Adsorbents	$Q_{m,cal}$ (mg g^{-1})	pH	T(K)	t(min)	Year	Ref.
MI-FDU-12	363.5	3.0	298	40	2023	This study
	385.5	3.0	298	40		
	409.0	3.0	298	40		
	416.9	3.0	298	40		
MCB-ECH-SH/SO_3H	293.5	5.0	333	–	2023	[51]
ANZ–Fe_3O_4	~2.8	2.0	298	50	2022	[52]
IIP@GO-Fe_3O_4	8.5	2.0	323	40	2021	[53]
MgAl/LDH-PBC	177.9	2.0	308	180	2023	[54]
MS-HMS-PL	257.7	4.0	293	90	2020	[55]
MI-Cl-KCC-1	428.0	3.0–4.0	298	40	2020	[27]
IIP	~1.3	2.0	313	30	2020	[56]
MSP	53.6	2.0	298	120	2019	[57]
PANI@NC nanocomposites	198.0	1.0	298	480	2019	[58]
IIP-ANZ	~4.4	2.0	303	30	2018	[59]
NMA-LDOs	103.4	–	303	150	2017	[60]
Fe_3O_4/GO	32.3	4.5	293	300	2013	[61]
G–MgAl-LDH nanocomposite	172.5	2.0	293	24 h	2013	[62]
MHCSs	200	3.0	298	~700	2013	[63]
bismuth hollow nanospheres	17.5	2.0	RT	–	2012	[64]
EMCMCR	51.8	2.0	293	6–10	2011	[65]
MCS	200	natural	303	60	2011	[66]
Chitosan flakes	102	3.0	293	–	2009	[67]
magnetic poly (GMA–EGDMA) beads	140.6	2.0	298	120	2008	[68]

4. Conclusion

In conclusion, this study introduces an innovative eco-design approach for the synthesis of a highly efficient Cr(VI) anion-exchange adsorbent, namely MI-Cl-FDU-12, by utilizing a positively charged surface mesoporous silica material. The synthesis method employed a one-pot synthesis protocol that incorporated environmentally friendly sodium silicate extracted from sorghum waste as a green silica source and M−TESP−IC as a functionalization agent. The resulting MI-Cl-FDU-12 adsorbent exhibited an well-ordered bimodal micro-/mesoporous structure with a high surface area of 672 m^2 g^{-1}, window size of 1.2 nm, cavity diameter of 7.5 nm, and total pore volume of 0.72 m^3 g^{-1}, comparable to previous reports on FDU-12 synthesis. MI-Cl-FDU-12 exhibited remarkable adsorption capabilities for the removal of toxic Cr(VI) from aqueous solution. The adsorption behavior of Cr(VI) on the MI-Cl-FDU-12 adsorbent was analyzed using various kinetic models (the effect of contact time) and isotherm models (the effect of initial concentration of adsorbate) after optimization of pH and adsorbent dose. The Langmuir model provided the best fit to the experimental data at four different temperatures, suggesting a homogeneous surface site affinity. The theoretical maximum adsorption capacities of MI-Cl-FDU-12 were found to exceed those of most previously reported Cr(VI) adsorbents in the literature, reaching values of 363.5, 385.5, 409.0, and 416.9 mg g^{-1} at 298, 303, 308, and 313 K, respectively, under optimal

conditions (pH=2, W=3 mg, and t=30 min). Furthermore, MI-Cl-FDU-12 exhibited excellent regeneration performance, retaining its outstanding adsorption properties even after six consecutive recycling cycles. This highlights the potential of MI-Cl-FDU-12 as a sustainable and durable adsorbent for Cr(VI) removal in water remediation applications. Further research and optimization of the MI-Cl-FDU-12 adsorbent could lead to its practical implementation in real-world water treatment systems, addressing the pressing challenges of water pollution and ensuring the availability of clean water resources.

CRediT authorship contribution statement

Saeed Shirazian: Writing – review & editing, Validation, Project administration, Methodology, Funding acquisition, Formal analysis. **Thoa Huynh:** Writing – review & editing, Validation, Methodology, Formal analysis, Data curation, Conceptualization. **Niloofar Pirestani:** Writing – review & editing, Writing – original draft, Visualization, Software, Methodology, Investigation, Formal analysis. **Roozbeh Soltani:** Writing – review & editing, Writing – original draft, Visualization, Supervision, Software, Project administration, Methodology, Investigation, Formal analysis, Conceptualization. **Azam Marjani:** Writing – review & editing, Validation, Methodology, Formal analysis, Data curation, Conceptualization. **Ahmad B. Albadarin:** Writing – review & editing, Validation, Software, Methodology, Conceptualization. **Shaheen M. Sarkar:** Writing – review & editing, Investigation, Formal analysis, Data curation.

Declaration of competing interest

The authors declare that they have no known competing financial interests or personal relationships that could have appeared to influence the work reported in this paper.

Data availability

Data will be made available on request.

References

[1] A.B. Albadarin, Z. Yang, C. Mangwandi, Y. Glocheux, G. Walker, M.N.M. Ahmad, Experimental design and batch experiments for optimization of Cr(VI) removal from aqueous solutions by hydrous cerium oxide nanoparticles, Chem. Eng. Res. Design. 92 (2014), https://doi.org/10.1016/j.cherd.2013.10.015.

[2] R.T. Kapoor, M.F. Bani Mfarrej, P. Alam, J. Rinklebe, P. Ahmad, Accumulation of chromium in plants and its repercussion in animals and humans, Environ. Pollut. 301 (2022), https://doi.org/10.1016/j.envpol.2022.119044.

[3] A.K. Shanker, C. Cervantes, H. Loza-Tavera, S. Avudainayagam, Chromium toxicity in plants, Environ. Int. 31 (2005), https://doi.org/10.1016/j.envint.2005.02.003.

[4] R. Soltani, R. Pelalak, M. Pishnamazi, A. Marjani, A.B. Albadarin, S.M. Sarkar, S. Shirazian, Synthesis of multi-organo-functionalized fibrous silica KCC-1 for highly efficient adsorption of acid fuchsine and acid orange II from aqueous solution, Sci. Rep. 11 (2021), https://doi.org/10.1038/s41598-021-81080-3.

[5] R. Soltani, M. Pishnamazi, R. Pelalak, M. Rezakazemi, A. Marjani, M. Dinari, S. M. Sarkar, S. Shirazian, Preparation of COOH-KCC-1/polyamide 6 composite by in situ ring-opening polymerization: Synthesis, characterization, and Cd(II) adsorption study, J. Environ. Chem. Eng. 9 (2021), https://doi.org/10.1016/j.jece.2020.104683.

[6] N. Musa, B.K. Allam, N.B. Singh, S. Banerjee, Investigation on water defluoridation via batch and continuous mode using Ce–Al bimetallic oxide: Adsorption dynamics, electrochemical and LCA analysis, Environ. Pollut. 328 (2023), https://doi.org/10.1016/j.envpol.2023.121639.

[7] N. Musa, B. Kumar Allam, S. Sajad, N. Bahadur Singh, S. Banerjee, Synthesis, characterization, and phytotoxicity evaluation of Ce/Zr bimetallic oxides as adsorbents for nitrate decontamination from water, Groundw, Sustain. Dev. 23 (2023) 101034, https://doi.org/10.1016/j.gsd.2023.101034.

[8] J.O. Ighalo, F.O. Omoarukhe, V.E. Ojukwu, K.O. Iwuozor, C.A. Igwegbe, Cost of adsorbent preparation and usage in wastewater treatment: A review, Clean. Chem. Eng. 3 (2022), https://doi.org/10.1016/j.clce.2022.100042.

[9] M. Ponnuchamy, A. Kapoor, P. Senthil Kumar, D.V.N. Vo, A. Balakrishnan, M. Mariam Jacob, P. Sivaraman, Sustainable adsorbents for the removal of pesticides from water: a review, Environ. Chem. Lett. 19 (2021), https://doi.org/10.1007/s10311-021-01183-1.

[10] M. Bilal, I. Ihsanullah, M. Younas, M. Ul Hassan Shah, Recent advances in applications of low-cost adsorbents for the removal of heavy metals from water: A critical review, Sep. Purif. Technol. 278 (2022), https://doi.org/10.1016/j.seppur.2021.119510.

[11] Y.A.B. Neolaka, Y. Lawa, J. Naat, A.C. Lalang, B.A. Widyaningrum, G.F. Ngasu, K. A. Niga, H. Darmokoesoemo, M. Iqbal, H.S. Kusuma, Adsorption of methyl red from aqueous solution using Bali cow bones (Bos javanicus domesticus) hydrochar powder, Results Eng. 17 (2023), https://doi.org/10.1016/j.rineng.2022.100824.

[12] H.S. Kusuma, N. Illiyanasafa, D. Engelien Christa Jaya, H. Darmokoesoemo, N. R. Putra, Utilization of the microalga Chlorella vulgaris for mercury bioremediation from wastewater and biomass production, Sustain. Chem. Pharm. 37 (2024) 101346, https://doi.org/10.1016/j.scp.2023.101346.

[13] S. Tavasolikejani, S.M. Hosseini, M. Ghiaci, T. Vangijzegem, S. Laurent, Copper nanoparticles embedded into nitrogen-doped carbon fiber felt as recyclable catalyst for benzene oxidation under mild conditions, Mol. Catal. 553 (2024) 113736, https://doi.org/10.1016/j.mcat.2023.113736.

[14] S. Tavasolikejani, A. Farazin, Explore the most recent advancements in the domain of self-healing intelligent composites specifically designed for use in dentistry, J. Mech. Behav. Biomed. Mater. 147 (2023), https://doi.org/10.1016/j.jmbbm.2023.106123.

[15] S. Tavasolikejani, A. Farazin, Fabrication and modeling of nanocomposites with bioceramic nanoparticles for rapid wound healing: An experimental and molecular dynamics investigation, Nanomedicine Res. J. 8 (2023) 412–429, https://doi.org/10.22034/nmrj.2023.04.010.

[16] A. Roghanizad, M. Karimi Abdolmaleki, S.M. Ghoreishi, M. Dinari, One-pot synthesis of functionalized mesoporous fibrous silica nanospheres for dye adsorption: Isotherm, kinetic, and thermodynamic studies, J. Mol. Liq. 300 (2020), https://doi.org/10.1016/j.molliq.2019.112367.

[17] S. Tavasolikejani, A. Farazin, The effect of increasing temperature on simulated nanocomposites reinforced with SWBNNs and its effect on characteristics related to mechanics and the physical attributes using the MDs approach, Heliyon. 9 (2023). https://www.cell.com/heliyon/pdf/S2405-8440(23)08230-0.pdf.

[18] Z.A. Alothman, A review: Fundamental aspects of silicate mesoporous materials, Materials (basel). 5 (2012) 2874–2902, https://doi.org/10.3390/ma5122874.

[19] E. Da'na, Adsorption of heavy metals on functionalized-mesoporous silica: A review, Microporous Mesoporous Mater. 247 (2017) 145–157, https://doi.org/10.1016/j.micromeso.2017.03.050.

[20] R. Soltani, A. Marjani, S. Shirazian, Novel mesoporous crumpled paper-like silica balls, Mater. Lett. 281 (2020), https://doi.org/10.1016/j.matlet.2020.128230.

[21] R. Soltani, M. Nazari, A. Marjani, M. Faisal, N. Pirestani, A.B. Albadarin, S. Soltani, C.H. Su, C.H. Chang, M. Pishnamazi, M.J. Ansari, S. Shirazian, Bio-based 3D dendritic silica nanosphere: A green superior adsorbent, J. Clean. Prod. 335 (2022), https://doi.org/10.1016/j.jclepro.2021.130204.

[22] C. Gérardin, J. Reboul, M. Bonne, B. Lebeau, Ecodesign of ordered mesoporous silica materials, Chem. Soc. Rev. 42 (2013), https://doi.org/10.1039/c3cs35451b.

[23] Crops and livestock products, Food Agric. Organ. United Nations. (n.d.). https://www.fao.org/faostat/en/#data/QCL.

[24] M. Ahmad Yahaya, H. Shimelis, B. Nebie, C.O. Ojiewo, G. Danso-Abbeam, Sorghum production in Nigeria: opportunities, constraints, and recommendations, Acta Agric, Scand. Sect. B Soil Plant Sci. 72 (2022), https://doi.org/10.1080/09064710.2022.2047771.

[25] J. Fan, C. Yu, F. Gao, J. Lei, B. Tian, L. Wang, Q. Luo, B. Tu, W. Zhou, D. Zhao, Cubic mesoporous silica with large controllable entrance sizes and advanced adsorption properties, Angew. Chemie - Int. Ed. 42 (2003) 3146–3150, https://doi.org/10.1002/anie.200351027.

[26] A. Vinu, K.Z. Hossain, K. Ariga, Recent advances in functionalization of mesoporous silica, J. Nanosci. Nanotechnol. 5 (2005) 347–371, https://doi.org/10.1166/jnn.2005.089.

[27] R. Soltani, A. Marjani, M. Hosseini, S. Shirazian, Synthesis and characterization of novel N-methylimidazolium-functionalized KCC-1: A highly efficient anion exchanger of hexavalent chromium, Chemosphere. 239 (2020), https://doi.org/10.1016/j.chemosphere.2019.124735.

[28] M.A. El-Sayed, T.M. El-Samni, Physical and Chemical Properties of Rice Straw Ash and Its Effect on the Cement Paste Produced from Different Cement Types, J. King Saud Univ. - Eng. Sci. 19 (2006), https://doi.org/10.1016/S1018-3639(18)30845-6.

[29] M. Balamurugan, S. Saravanan, Producing nanosilica from Sorghum vulgare seed heads, Powder Technol. 224 (2012), https://doi.org/10.1016/j.powtec.2012.03.017.

[30] J. Fan, C. Yu, L. Wang, B. Tu, D. Zhao, Y. Sakamoto, O. Terasaki, Mesotunnels on the silica wall of ordered SBA-15 to generate three-dimensional large-pore mesoporous networks [15], J. Am. Chem. Soc. 123 (2001), https://doi.org/10.1021/ja011564l.

[31] J.M. Kim, Y. Sakamoto, Y.K. Hwang, Y.U. Kwon, O. Terasaki, S.E. Park, G. D. Stucky, Structural design of mesoporous silica by micelle-packing control using blends of amphiphilic block copolymers, J. Phys. Chem. b. 106 (2002), https://doi.org/10.1021/jp014280w.

[32] S. Meoto, N. Kent, M.M. Nigra, M.O. Coppens, Effect of stirring rate on the morphology of FDU-12 mesoporous silica particles, Microporous Mesoporous Mater. 249 (2017), https://doi.org/10.1016/j.micromeso.2017.04.045.

[33] M.N. Sarvi, T. Budianto Bee, C.K. Gooi, B.W. Woonton, M.L. Gee, A.J. O'Connor, Development of functionalized mesoporous silica for adsorption and separation of dairy proteins, Chem. Eng. J. 235 (2014) 244–251, https://doi.org/10.1016/j.cej.2013.09.036.

[34] T. Yu, H. Zhang, X. Yan, Z. Chen, X. Zou, P. Oleynikov, D. Zhao, Pore structures of ordered large cage-type mesoporous silica FDU-12s, J. Phys. Chem. b. 110 (2006), https://doi.org/10.1021/jp064534j.

[35] I. Langmuir, The constitution and fundamental properties of solids and liquids. Part I. Solids, J. Am. Chem. Soc. 38 (1916) 2221–2295, https://doi.org/10.1021/ja02268a002.
[36] I. Langmuir, The adsorption of gases on plane surfaces of glass, mica and platinum, J. Am. Chem. Soc. 40 (1918), https://doi.org/10.1021/ja02242a004.
[37] H.M.F. Fruendlich, Over the adsorption in solution, J. Phys. Chem. 57 (1906) 385–471.
[38] M. Temkin, V. Pyzhev, Kinetics of Ammonia Synthesis on Promoted Iron Catalysts, Acta Physicochim. u.r.s.s. 12 (1940) 217–222.
[39] R.D. Johnson, F.H. Arnold, The temkin isotherm describes heterogeneous protein adsorption, Biochim. Biophys. Acta (BBA)/Protein Struct. Mol. (1995) 1247, https://doi.org/10.1016/0167-4838(95)00006-G.
[40] L.s. k, About the Theory of So-called Adsorption of Soluble Substances, Sven. Vetenskapsakad. Handingarl. 24 (1898) 1–39.
[41] H. Yuh-Shan, ADSORPTION OF HEAVY METALS EROM WASTE STREAMS BY PEAT School of Chemical Engineering, The University of Birmingham, 1995. https://etheses.bham.ac.uk//id/eprint/8742/1/Ho%2C Yuh-Shan_1995_PhD_01840180_%5BeTheses%5D.pdf.
[42] S.Y. Elovich, G.M. Zhabrova, Mechanism of the catalytic hydrogenation of ethylene on nickel. I. Kinetics of the process, Zhurnal Fiz. Khimii. 13 (1939) 1761–1775.
[43] M. Avrami, Kinetics of phase change. I: General theory, J. Chem. Phys. 7 (1939) 1103–1112, https://doi.org/10.1063/1.1750380.
[44] A.B. Albadarin, Y. Glocheux, M.N.M. Ahmad, G.M. Walker, C. Mangwandi, Novel comparison of kinetic models for the adsorption-coupled reduction of Cr(VI) using untreated date pit biomaterial, Ecological Eng. 70 (2014), https://doi.org/10.1016/j.ecoleng.2014.05.002.
[45] Y.S. Ho, W.T. Chiu, C.C. Wang, Regression analysis for the sorption isotherms of basic dyes on sugarcane dust, Bioresour. Technol. 96 (2005), https://doi.org/10.1016/j.biortech.2004.10.021.
[46] N. Ayawei, A.N. Ebelegi, D. Wankasi, Modelling and Interpretation of Adsorption Isotherms, J. Chem. 2017 (2017), https://doi.org/10.1155/2017/3039817.
[47] V. Patrulea, A. Negrulescu, M.M. Mincea, L.D. Pitulice, O.B. Spiridon, V. Ostafe, Optimization of the Removal of Copper(II) Ions from Aqueous Solution on Chitosan and Cross-Linked Chitosan Beads, BioResources. 8 (2013), https://doi.org/10.15376/biores.8.1.1147-1165.
[48] F. Batool, J. Akbar, S. Iqbal, S. Noreen, S.N.A. Bukhari, Study of Isothermal, Kinetic, and Thermodynamic Parameters for Adsorption of Cadmium: An Overview of Linear and Nonlinear Approach and Error Analysis, Bioinorg. Chem. Appl. 2018 (2018), https://doi.org/10.1155/2018/3463724.
[49] E.C.N. Lopes, F.S.C. Dos Anjos, E.F.S. Vieira, A.R. Cestari, An alternative Avrami equation to evaluate kinetic parameters of the interaction of Hg(II) with thin chitosan membranes, J. Colloid Interface Sci. 263 (2003), https://doi.org/10.1016/S0021-9797(03)00326-6.
[50] A.M.M. Vargas, A.L. Cazetta, M.H. Kunita, T.L. Silva, V.C. Almeida, Adsorption of methylene blue on activated carbon produced from flamboyant pods (Delonix regia): Study of adsorption isotherms and kinetic models, Chem. Eng. J. 168 (2011), https://doi.org/10.1016/j.cej.2011.01.067.
[51] L. Li, Q. Liao, B. Hou, C. He, J. Liu, B. Li, M. Yu, Y. Liu, B. Lai, B. Yang, Synchronous reduction and removal of hexavalent chromium from wastewater by modified magnetic chitosan beads, Sep. Purif. Technol. 304 (2023), https://doi.org/10.1016/j.seppur.2022.122363.
[52] Y.A.B. Neolaka, Y. Lawa, J. Naat, A.A.P. Riwu, A.W. Mango, H. Darmokoesoemo, B. A. Widyaningrum, M. Iqbal, H.S. Kusuma, Efficiency of activated natural zeolite-based magnetic composite (ANZ-Fe3O4) as a novel adsorbent for removal of Cr(VI) from wastewater, J. Mater. Res. Technol. 18 (2022), https://doi.org/10.1016/j.jmrt.2022.03.153.
[53] Y.A.B. Neolaka, Y. Lawa, J. Naat, A.A.P. Riwu, Y.E. Lindu, H. Darmokoesoemo, B. A. Widyaningrum, M. Iqbal, H.S. Kusuma, Evaluation of magnetic material IIP@GO-Fe3O4 based on Kesambi wood (Schleichera oleosa) as a potential adsorbent for the removal of Cr(VI) from aqueous solutions, React. Funct. Polym. 166 (2021), https://doi.org/10.1016/j.reactfunctpolym.2021.105000.
[54] X. Li, Z. Shi, J. Zhang, T. Gan, Z. Xiao, Aqueous Cr (VI) removal performance of an invasive plant-derived biochar modified by Mg/Al-layered double hydroxides, Colloids Interface Sci. Commun. 53 (2023), https://doi.org/10.1016/j.colcom.2023.100700.
[55] R. Soltani, A. Marjani, R. Soltani, S. Shirazian, Hierarchical multi-shell hollow micro–meso–macroporous silica for Cr(VI) adsorption, Sci. Rep. 10 (2020), https://doi.org/10.1038/s41598-020-66540-6.
[56] Y.A.B. Neolaka, Y. Lawa, J.N. Naat, A.A. Pau Riwu, H. Darmokoesoemo, G. Supriyanto, C.I. Holdsworth, A.N. Amenaghawon, H.S. Kusuma, A Cr(VI)-imprinted-poly(4-VP-co-EGDMA) sorbent prepared using precipitation polymerization and its application for selective adsorptive removal and solid phase extraction of Cr(VI) ions from electroplating industrial wastewater, React. Funct. Polym. 147 (2020), https://doi.org/10.1016/j.reactfunctpolym.2019.104451.
[57] M. Mobarak, E.A. Mohamed, A.Q. Selim, L. Sellaoui, A. Ben Lamine, A. Erto, A. Bonilla-Petriciolet, M.K. Seliem, Surfactant–modified serpentine for fluoride and Cr(VI) adsorption in single and binary systems: Experimental studies and theoretical modeling, Chem. Eng. J. 369 (2019) 333–343, https://doi.org/10.1016/j.cej.2019.03.086.
[58] Y. Lai, F. Wang, Y. Zhang, P. Ou, P. Wu, Q. Fang, Z. Chen, S. Li, UiO-66 derived N-doped carbon nanoparticles coated by PANI for simultaneous adsorption and reduction of hexavalent chromium from waste water, Chem. Eng. J. 378 (2019), https://doi.org/10.1016/j.cej.2019.122069.
[59] Y.A.B. Neolaka, G. Supriyanto, H.S. Kusuma, Adsorption performance of Cr(VI)-imprinted poly(4-VP-co-MMA) supported on activated Indonesia (Ende-Flores) natural zeolite structure for Cr(VI) removal from aqueous solution, J. Environ. Chem. Eng. 6 (2018), https://doi.org/10.1016/j.jece.2018.04.053.
[60] C. Lei, X. Zhu, B. Zhu, C. Jiang, Y. Le, J. Yu, Superb adsorption capacity of hierarchical calcined Ni/Mg/Al layered double hydroxides for Congo red and Cr (VI) ions, J. Hazard. Mater. 321 (2017) 801–811, https://doi.org/10.1016/j.jhazmat.2016.09.070.
[61] M. Liu, T. Wen, X. Wu, C. Chen, J. Hu, J. Li, X. Wang, Synthesis of porous Fe3O4 hollow microspheres/ graphene oxide composite for Cr(vi) removal, Dalt. Trans. 42 (2013) 14710–14717, https://doi.org/10.1039/c3dt50955a.
[62] X. Yuan, Y. Wang, J. Wang, C. Zhou, Q. Tang, X. Rao, Calcined graphene/MgAl-layered double hydroxides for enhanced Cr(VI) removal, Chem. Eng. J. 221 (2013) 204–213, https://doi.org/10.1016/j.cej.2013.01.090.
[63] L.H. Zhang, Q. Sun, D.H. Liu, A.H. Lu, Magnetic hollow carbon nanospheres for removal of chromium ions, J. Mater. Chem. a. 1 (2013) 9477–9483, https://doi.org/10.1039/c3ta10430c.
[64] F. Qin, G. Li, H. Xiao, Z. Lu, H. Sun, R. Chen, Large-scale synthesis of bismuth hollow nanospheres for highly efficient Cr(vi) removal, Dalt. Trans. 41 (2012) 11263–11266, https://doi.org/10.1039/c2dt31021j.
[65] X. jiang Hu, J. song Wang, Y. guo Liu, X. Li, G. ming Zeng, Z. lei Bao, X. xia Zeng, A. wei Chen, F. Long, Adsorption of chromium (VI) by ethylenediamine-modified cross-linked magnetic chitosan resin: Isotherms, kinetics and thermodynamics, J. Hazard. Mater. 185 (2011) 306–314, https://doi.org/10.1016/j.jhazmat.2010.09.034.
[66] S. Chen, Q. Yue, B. Gao, Q. Li, X. Xu, Removal of Cr(VI) from aqueous solution using modified corn stalks: Characteristic, equilibrium, kinetic and thermodynamic study, Chem. Eng. J. 168 (2011) 909–917, https://doi.org/10.1016/j.cej.2011.01.063.
[67] Y.A. Aydin, N.D. Aksoy, Adsorption of chromium on chitosan: Optimization, kinetics and thermodynamics, Chem. Eng. J. 151 (2009) 188–194, https://doi.org/10.1016/j.cej.2009.02.010.
[68] G. Bayramoğlu, M. Yakup Arica, Adsorption of Cr(VI) onto PEI immobilized acrylate-based magnetic beads: Isotherms, kinetics and thermodynamics study, Chem. Eng. J. 139 (2008) 20–28, https://doi.org/10.1016/j.cej.2007.07.068.